

# Corroded Post-Tensioned Concrete Beams Fatigue Behavior Under High Cyclic Loading

Mohammad Mahdi Sultani<sup>1\*</sup>, Liang Dong<sup>1</sup>, Ge Changwei<sup>1</sup>

<sup>1</sup> School of Civil and Transportation Engineering, Hebei University of Technology, Tianjin 300401, China

Received 15 March 2022; Accepted 29 March 2022

**Abstract:** Corrosion of tension wires in bonded post-tensioned concrete beams accelerates fatigue damage accumulation and shortens fatigue lifespan significantly. In this article, the fatigue behavior of post-tensioned concrete beams is studied experimentally under varying strand corrosion levels and high cyclic loading. An accelerated corrosion test is conducted in order to acquire varied corroded beam specimens. First, eight test beams were designed, and one of them was statically tested. Furthermore, the fatigue amplitude was determined using static test results. The remaining seven beams with various corrosion degrees were subjected to constant amplitude high cyclic fatigue loading tests. The test findings reveal that as the corrosion level rises, the failure mechanism shifts from non prestressed steel bar fracture to prestressed steel strand breaking. And under high cyclic loading, fatigue cracks initiate and propagate rapidly around corrosion pits. prestressing wires exhibited fatigue fractures at the minimal cross-sections where corrosion pits had grown. Consequently, a fatigue load test was used to investigate load-deflection, crack propagation, and fatigue life in PC beams after multiple high fatigue cycles, and corrosion-induced cracking is discussed experimentally. Overall, it was observed that corrosion shortens the fatigue life and degrades the stiffness, increasing deflection and crack widths faster than uncorroded beams under high cyclic fatigue loading.

**Keywords:** Post-tensioned concrete, Corrosion level, Fatigue fracture, Corrosion induced cracking

## I. INTRODUCTION

Prestressing steel corrosion has long been acknowledged as a global issue that has resulted in significant structural damage and deterioration. Corrosion products take up more space, causing strains in the cover concrete, which can lead to cracking, delamination, and spalling. During the service life, approximately 55–65% of the steel's ultimate tensile strength is constantly applied to pre-stressed steel [1, 2]. The steel strand's tensile strength and ductility will be reduced as a result of cross-sectional area loss owing to corrosion and Local yielding and fracture are the most common outcomes. As evidenced by the unexpected collapses of the Ynys-y-Gwas bridge in the UK and the Saint Stefano bridge in Italy, prestressed steel failure can result in brittle fracture of structural elements as well as the potential of the bridge falling totally [3, 4]. Expensive restoration of these degraded structures is required to prevent further damage. According to the report, in the United States, one out of every nine bridges is deemed structurally poor, and repairing them will cost \$20.5 billion every year [5]. Numerous studies have been conducted on the static flexural performance of prestressed concrete beams with corroded prestressing steel. Corroded prestressing steel invariably fails in tensile testing at the minimal cross-sectional area, resulting in severe deformability and a loss of load capacity [6-9]. Pull-out tests have also revealed that the bond between corroded prestressing strands and concrete has deteriorated. [10-12]. Static tests on corroded prestressed concrete beams revealed significant deformation and load capacity loss, as well as an early brittle failure mechanism [13]. Corrosion pits were discovered at random throughout the length of a steel bar, with the disparity between the minimum and average cross-sectional area increasing as corrosion increased [14]. Additional research found that corroded prestressed concrete beams might fracture at cross-sections not subjected to the maximum moment, which the likelihood of failure for both strength and serviceability increases [15].

During their service life, bridges made of prestressed concrete are similarly prone to fatigue. The bottom prestressed steel of bridge girders experiences cyclic stress fluctuations that are rather frequent due to traffic loads. The corrosion sensitivity of fatigue behavior is greater than that of static tensile behavior, according to high-cycle tension fatigue tests on corroded steel bars, as well as the fact that corrosion shortens fatigue life significantly [9, 16]. Nonetheless, when chloride corrosion and fatigue loading combine, these components have a reciprocal influence, resulting in a coupling effect that drastically lowers the operating ability of the prestressed concrete structure. Experiments on the mechanical properties of corroded prestressed steel wire under high-cycle fatigue load were also carried out, and based on the findings, due to uneven corrosion, all corroded prestressing wires failed around corrosion pits, and as the degree of corrosion and the number of loading cycles

grew, the ultimate strength and strain of corroded prestressing wires decreased drastically [17-19]. Bridges with high levels of stress usually require pre-tensioned type and post-tensioned type concrete girders.

Furthermore, the number of publications have focused on the fatigue behavior of corroded pre-tensioned and reinforced concrete beams under mild cyclic loading [20-24], and according to the author's knowledge, few fatigue studies on corroded prestressed concrete beams of the post-tensioned type with high cyclic loading have been conducted. Furthermore, existing results on the fatigue behavior of post-tensioned type beams with corroded strands are insufficient, and the fatigue damage process is not well characterized. As a result, greater research and study into the fatigue behavior of post-tensioned concrete beams with corroded strands is required. In this paper, we present an experimental investigation of the fatigue performance of post-tensioned concrete beams with different levels of corrosion. Initially, a total of eight post-tensioned concrete beams were created, and six of them were corroded through the impressed current method. Furthermore, the fatigue behaviors of PC beams with corroded prestressing wire are such as, mechanisms of failure, mid-span displacement, fatigue cracks, bending stiffness, and strains in classical materials investigated. Moreover, corrosion-induced cracking is also analysed and discussed experimentally.

## II. EXPERIMENTAL PROGRAM

### 2.1. Specimens Design and Fabrication

A total of eight post-tensioned concrete beams are designed and constructed. The beams are all  $300 \times 350 \times 2500$  mm in size. Two 10 mm simple bars at the bottom, two 12 mm deformed bars at the top, and 10 mm stirrups placed at 100 mm intervals reinforce the beams. The beams are cast with a 32 mm concrete duct and stressed with a 15.2 mm seven-wire strand. C50 types of concrete have been used. The strand's initial prestress is 1395 MPa, which is approximately 0.75 times of its yield strength. Through the channels at the ends of the beams, grout was injected into the duct. Fig. 1 shows the details. Before the beams were built, the strands and reinforcing bars were evaluated for tensile strength. The prestressing strand's average yield strength was 1830 MPa. For the 12 mm deform bars, the average yield strength was 400 MPa, and for the 10 mm plain bars, it was 335 MPa. The concrete mixture contained 416 kg/m<sup>3</sup> of Portland cement. The coarse aggregate had a weight ratio of 1.6 to the fine aggregate. The water-cement ratio (w/c) is 0.46.

The beams were simply supported and loaded at two symmetrical four-point loads with a span of 2200 mm. As a point of reference, two beams were left in normal environmental conditions, while the strands of the other six beams were artificially corroded up to mass losses of 10%, 15%, 20%, 25%, 30%, and 35%, respectively. To determine the ultimate load capacity, one uncorroded beam was tested under static loading, in order to estimate the fatigue tests' minimum and maximum loads. One uncorroded and six corroded beams were evaluated under cyclic loading at a constant load range. The degree of corrosion was measured by gravimetric mass loss to simplify engineering applications.

### 2.2. Accelerated corrosion process

A method of artificially accelerated corrosion testing is used. The corrosion region is 150 mm distant from each side of the mid-span corrosion area. The strand corrosion was electro-chemically accelerated after 28 days of concrete cure to get varied area losses. An epoxy cloth coating was employed to protect stirrups and longitudinal rebars from corroding. The corrosion system was composed of a direct current galvanostat, a strand anode, as well as a stainless steel cathode submerged in a 5% saline solution. A special corrosion tank was created and attached along the beam to prevent strand ends from being buried in the salty solution. Prior to the electrolytic corrosion, the beams were immersed in a saline solution for three days to aid in the corrosion process. A constant current density of 250 A/cm<sup>2</sup> was applied [25].

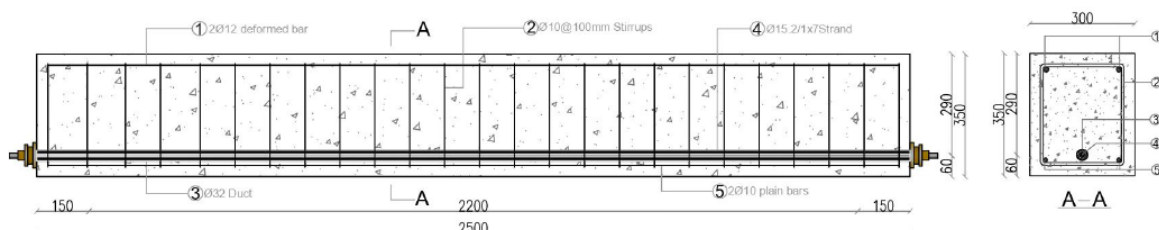


Fig. 1. Beam Details (Unit: mm)

For the different corrosion levels of the strands in the beams, different durations of impressed current were used based on Faraday's law. The schematic layout of the accelerated corrosion system is shown in Fig. 2. The duration of the corrosion process was determined by Faraday's law, in order to achieve the desired suitably corrected with a scale factor  $\alpha \geq 1$ , to consider the corrosion process's time lag, due to the protection provided by the concrete cover [26]. Faraday's law can be expressed in the following way.

$$\text{Time} = \alpha \frac{M_{\text{loss}} \cdot n_{\text{specimen}} \cdot C_{\text{Far}}}{I_{\text{corr}} \cdot M_{\text{specimen}}} \quad (1)$$

$M_{\text{specimen}}$  is the strands' molar mass,  $n_{\text{specimen}}$  is the valence,  $C_{\text{Far}}$  is the constant of Faraday (96,480 C.mol<sup>-1</sup>),  $I_{\text{corr}}$  is the imposed current expressed in amperes (A) and time is measured in seconds.

### 2.3. Corrosion induced cracking

Following the accelerated corrosion, the corrosion-induced cracking of PC beams was studied. On the side and bottom surfaces of the corroded beams, longitudinal cracks were detected. Cracks for the slightly corroded beam PCB4 is shown in Fig. 3. Along the beams, the cracks are almost interconnected. The corrosion-induced cracks varied in width across the beam. Near the cracks, some rust spots appear.

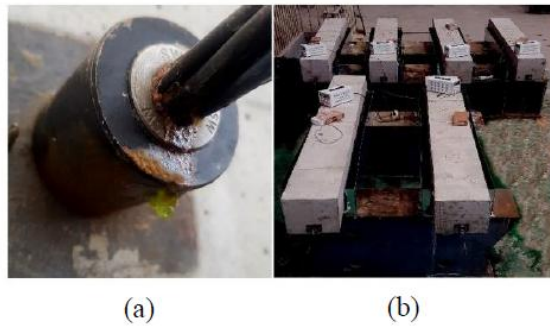


**Fig. 2.** (a) Corrosive liquid on anchoring zones  
(b) arrangement of accelerated corrosion system

Beam CB4 has a similar crack morphology to other corroded beams. An electric crack detector with high precision was used to measure the width of corrosion-induced cracks every around 7cm length. The average crack widths on the sides and bottom from all corroded beams are depicted in Fig 4. Increasing strand corrosion levels caused these cracks to widen. The bottom cracks were wider than those on the side surfaces due to the thin concrete covering. In beams PCB3 and PCB4, the crack width was consistent across the longitudinal axis.



**Fig. 3.** Corrosion-induced cracks in beam PCB4

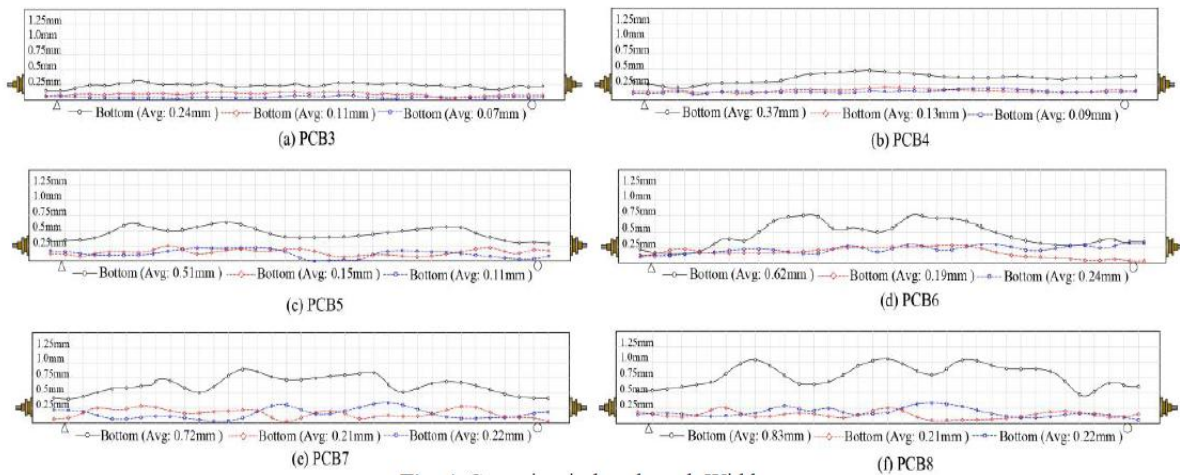


**Fig. 4. Corrosion-induced crack Width**

**2.4. Setup and loading procedures for the test**

The fatigue tests were conducted on the MTS electro-hydraulic servo-controlled fatigue-testing equipment, which includes a computerized system with seven test beams. Figs. 5 and 6 show the details of the fatigue test setup. To precisely determine the fatigue test load, the reference beam PCB1, which was free of corrosion, was monotonically tested to failure to determine the first cracking load  $P_{cr}$  and the ultimate load  $P_u$ . The remaining seven beams were subjected to cyclic loading with lower and maximum limits of 0.1  $P_u$  and 0.40  $P_u$ . The static load was applied before the cyclic loading began, and the load was steadily raised until it reached to  $P_{max}$ , it was then reduced to zero. Crack load, initial deflection, strain, and crack width were all taken into account and recorded. Then, at a frequency of 5 Hz, the load was applied in a cyclic pattern with a constant load range. After a certain number of cycles, the cyclic loading was stopped, 10,000, 20,000, 50,000, 70,000, 100,000, 150,000, 200,000, 300,000, 500,000, and 1 million respectively. Then fatigue loading test paused when the repeated cycles reached every step, and to assess the status of the beam a static cycle was performed between zero and  $P_{max}$ . Each time the fatigue testing was paused for static loading, data was taken from all of the equipment. During static loading, the crack width was also measured.

**2.5. Measurement of corrosion degree and Strand corrosion characteristic**

The flow of red rust and saline solution can be facilitated by the gaps between the twisted wires. Liquid migration has a negative impact on the structural lifespan and might cause corrosion to spread throughout the strand, as seen in Fig. 2. Corrosion loss in the strands of each beam was measured using a destructive technique. After the loading test, the concrete covering was removed, the strands were taken out, and the grout from their surfaces was wiped down. Corroded strands were cleansed with a 12 percent hydrochloric acid solution and neutralized with alkali. Corrosion is observed as the strand is separated into wires. A contour gauge was used after this to determine the remaining cross-sectional area of each wire.

This corrosion was almost completely concentrated on the external wires, the wire in the center is slightly corroded. Furthermore, the strand corrosion loss was computed using the areas of all wires in the same segment that were measured. Table 1 shows the maximum cross-section losses for each beam. The corrosion loss ranges from 10% to 35%.

For this study, corrosion loss of less than 15 % is considered minor corrosion (beams PC3 and PC4). Corrosion loss of 15-25 % is considered moderate (beams PC5 and PC6). Corrosion loss of more than 30 % is classified as severe (beams PC7 and PC8).

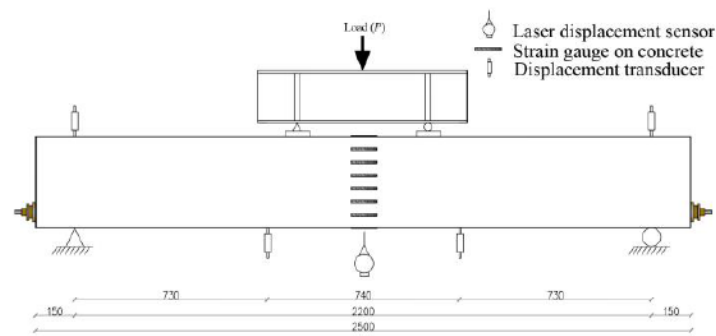


**Fig. 5.** Loading test set-up (Unit: mm)



**Fig. 6.** fatigue test setup

**Table 1.** Corrosion Levels of beams

Beam Name	PCB1	PCB2	PCB3	PCB4	PCB5	PCB6	PCB7	PCB8
Corrosion Level	0	0	10%	15%	20%	25%	30%	35%

**Table 2.** Failure mode, First crack load and fatigue life of the fatigue test beams

Beam No	Failure mode	First Crack Load $P_{cr}$ (kN)	Fatigue Life/Cycle ( $\times 10^4$ )	Load range of $P_{max}$
PCB2	fracture of bottom tensile steel bar	74	105.8	$0.40P_u$
PCB3	fracture of bottom tensile steel bar	71.2	101.4	$0.40P_u$
PCB4	Wire's breaking of steel strand	67.8	92.2	$0.40P_u$
PCB5	Wire's breaking of steel strand	63.1	79.9	$0.40P_u$
PCB6	Wire's breaking of steel strand	58.9	64.3	$0.40P_u$
PCB7	Wire's breaking of steel strand	52.7	41.1	$0.40P_u$
PCB8	Wire's breaking of steel strand	43.8	13.7	$0.40P_u$

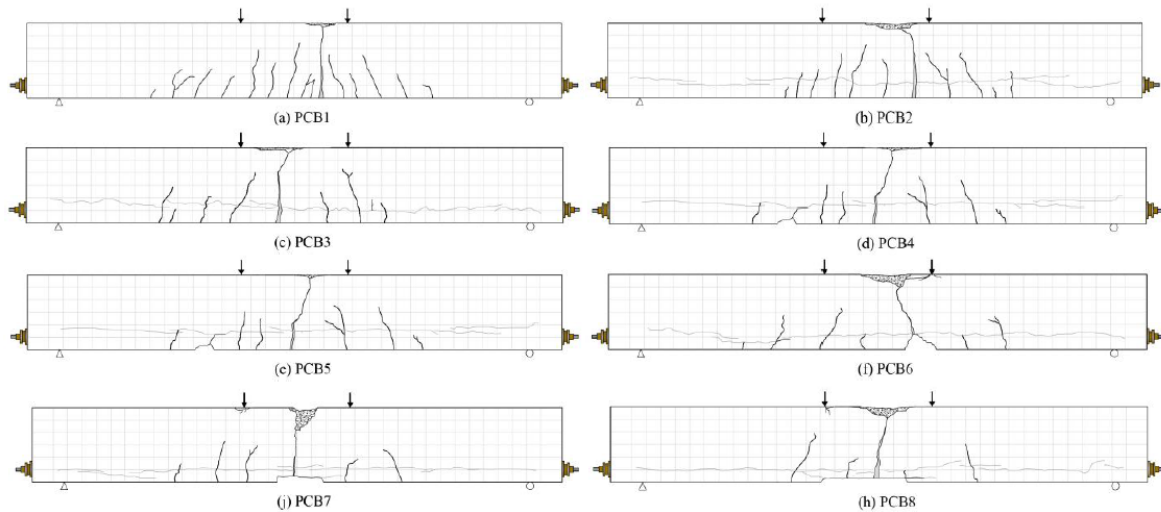


**Fig. 7.** Failure modes of beams in fatigue tests

### III. FATIGUE FAILURE MECHANISM OF TEST BEAMS

A static loading test was done on the beam PCB1 as a reference beam prior to the fatigue test. The ultimate load capacity of the beam PCB1 as tested was 229 kN, Then, using the control beam PCB1 load level as a guide, the minimum and maximum loads for the remaining seven beams in fatigue testing were determined. Table 2 describes the failure modes of and fatigue life of the test beam seven beams that failed by fatigue tests. fatigue failure for uncorroded beam PCB2 as reference beam caused by a sudden brittle fracture of longitudinal reinforcement. Longitudinal rebars are far away from the neutral axis, their initial stress range is greater than that of prestressing wires.

Therefore, fatigue failures occurred due to fatigue fracturing of rebars in uncorroded beams. As a result, for PCB2 approximately 1058010 cycles, the rebar fracturing occurred, and the beam promptly collapsed in a brittle state. This corresponds to previous findings [27]. Both rebars failed at the main crack, and there were no obvious signs of plastic deformation at the fracture surface. Fatigue cracks occurred and propagated rapidly around corrosion pits in corroded prestressing wires under cyclic loading. Under the same fatigue loading, corroded prestressing wires fractured before uncorroded tension rebars. Despite the fact that the wires had a lower nominal stress range. The remaining prestressing wires and rebars were fatigue fracturing in order till the beams collapsed brittlely. At the minimal cross-section, the first prestressing wire fractured, where there have been corrosion pits. Fig.7 illustrates the failed beams. Table 2 demonstrates the test beams' fatigue lifespan. As can be observed, the fatigue life drops dramatically as the corrosion level rises. The fatigue life span of the beams PCB3–PCB6 are 95.84%, 87.15%, 75.52, and 60.77% of that of the reference beam PCB2, respectively. The fatigue cycles at failure for the severely corroded beams PCB7 and PCB8 were 411000 and 137000, respectively, which are only 38.84% and 12.94% of the uncorroded beam. This is due to the fact that corrosion decreases the stand wire's net section area while raising the nominal stress amplitude. Fatigue failure is hastened by corrosion pit-induced stress concentration and covers spalling. Fracture analysis is one of the most extensively utilized approaches for analyzing the causes of fatigue crack development and propagation. The steel bar's fracture morphology is divided into two regions. A slow-expanding zone and steady fatigue crack growth region.

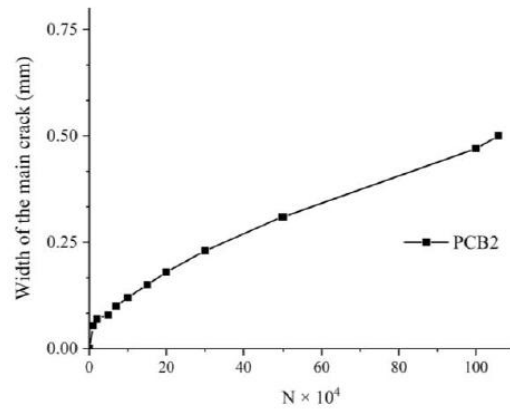
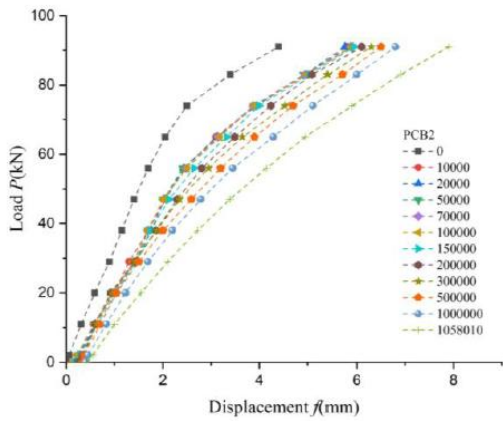
From the reinforcing surface to the radial direction, the fatigue crack takes on an arc form. Under fatigue load, the fracture of corroded strand wire is detected in the greatest corrosion pit position. As corrosion levels rise, the length of the stable fatigue crack development zone reduces. Corrosion accelerates the fatigue damage process by causing the Strand wire to reach the fast-expanding stage earlier.

#### 3.1 Load deflection after different fatigue cycles

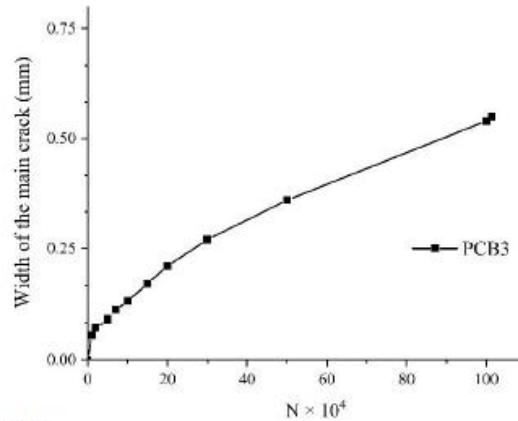
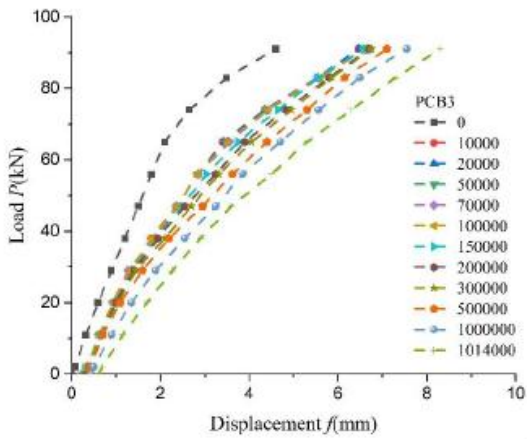
To find out how corrosion and fatigue impact the mechanical behavior of PC beams. Once the fatigue cycles have reached the required levels, the mid-span deflection is measured, as shown in Fig. 8. Strand wire's strength and cross-section are reduced by corrosion, particularly in severely cracked beams PCB7 and PCB8, and results in a reduction in the bond between strand wire and concrete. Fatigue reduces the flexural rigidity of PC beams, as can be shown. The flexural stiffness of PC beams degrades as a result of fatigue. Furthermore, after the same number of fatigue cycles as the virgin beam, the measured deflection increases. As the corrosion-induced fracture width rises, the distance between the deflection curves of various beams under different loads rises revealing that for the same cycle, structural stiffness is more susceptible to the width of corrosion cracking. The initial maximum deflections of PCB3–PCB8 beams increase by 10.23%, 22.1%, 42.03%, 53.01%, 69.51%

*Corroded Post-Tensioned Concrete Beams Fatigue Behaviour Under High Cyclic Loading*

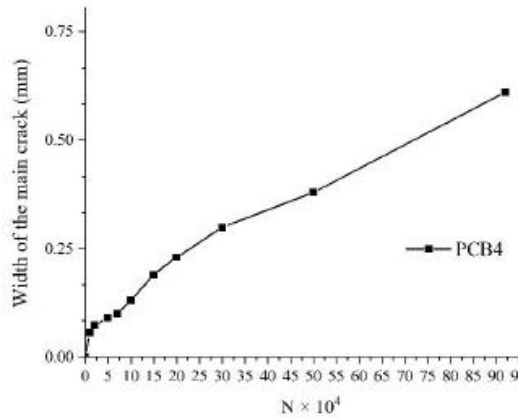
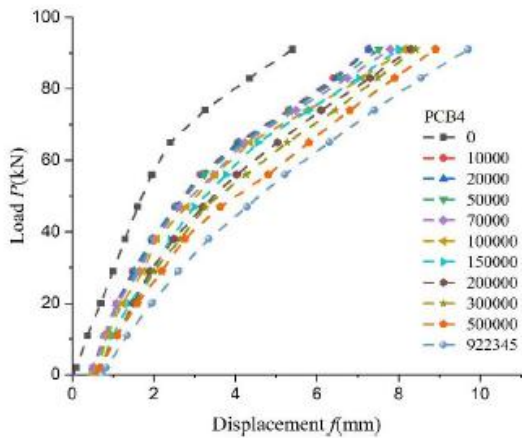
and 85.67%, respectively, when compared to the un-corroded beam. And as it seems under cyclic loading, mid-span deflection and strain gradually increased. The corroded beams exhibited more deflection, wider cracks, and greater strain under cyclic loading than the uncorroded beams.



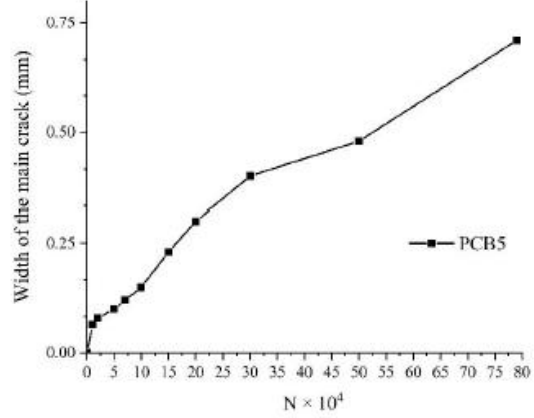
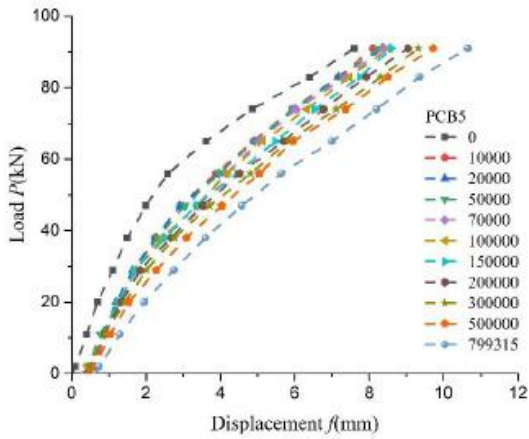
(a) PCB2



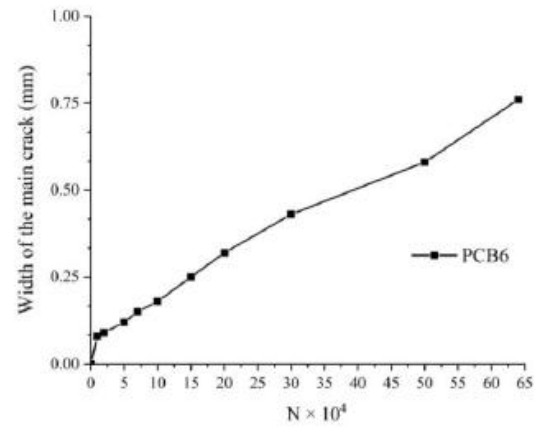
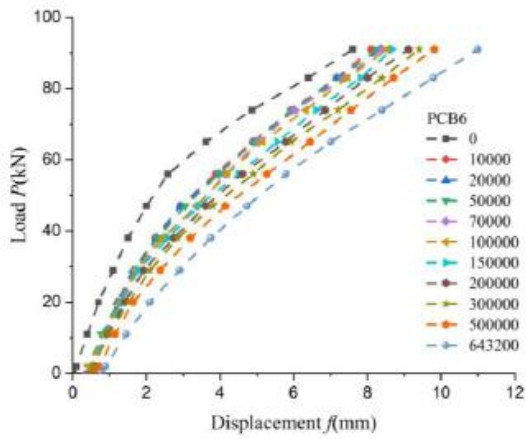
(b) PCB3



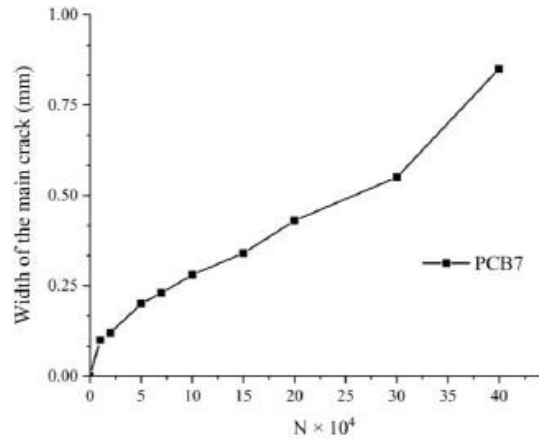
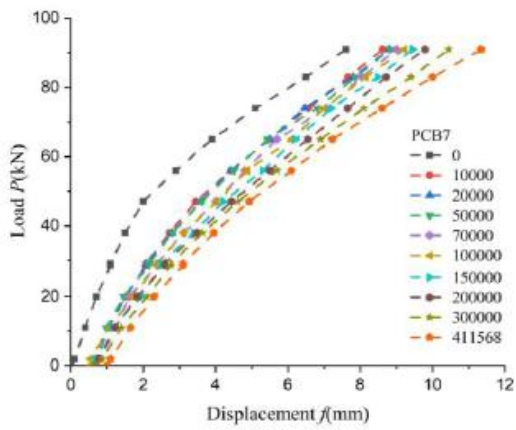
(c) PCB4



(d) PCB5



(e) PCB6



(f) PCB7

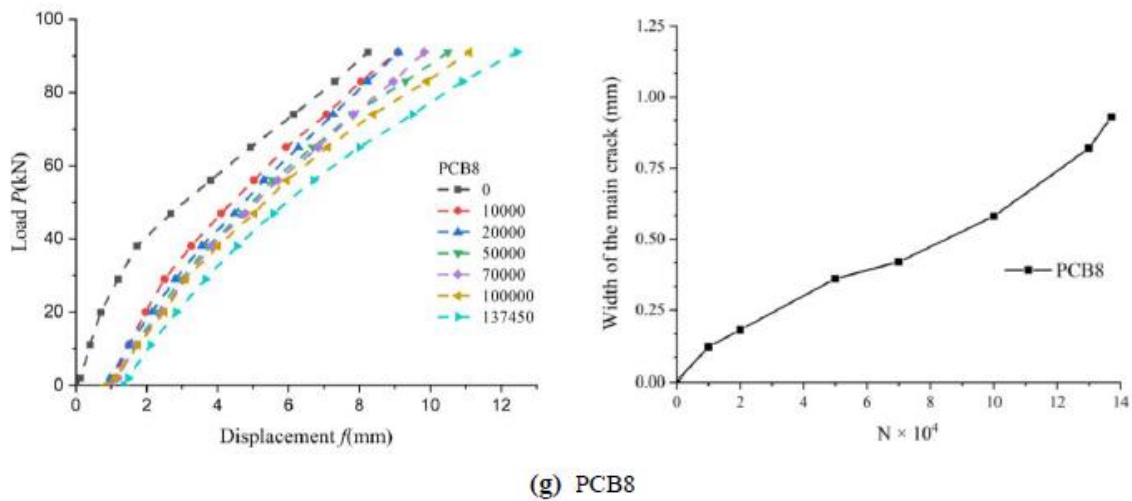


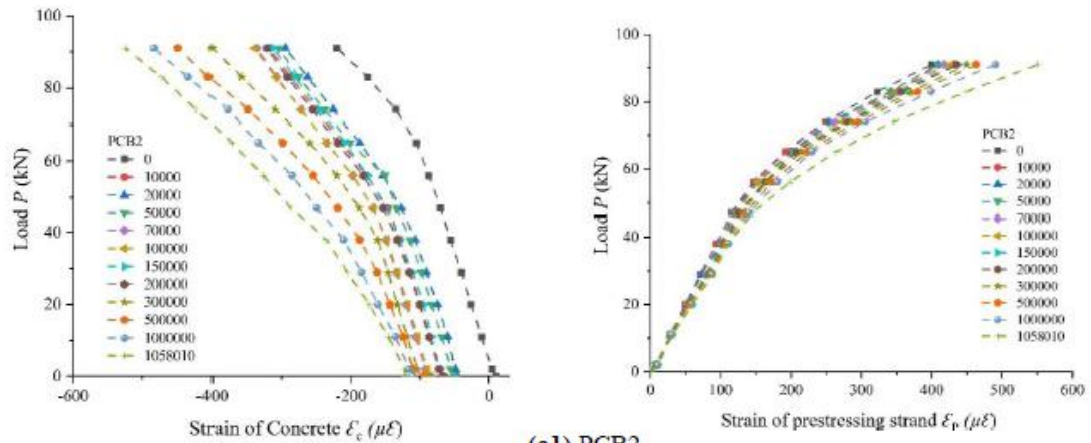
Fig. 8. Load midspan deflection curve and Crack Width (Unit: mm)

### 3.2 Displacement and main crack's progression

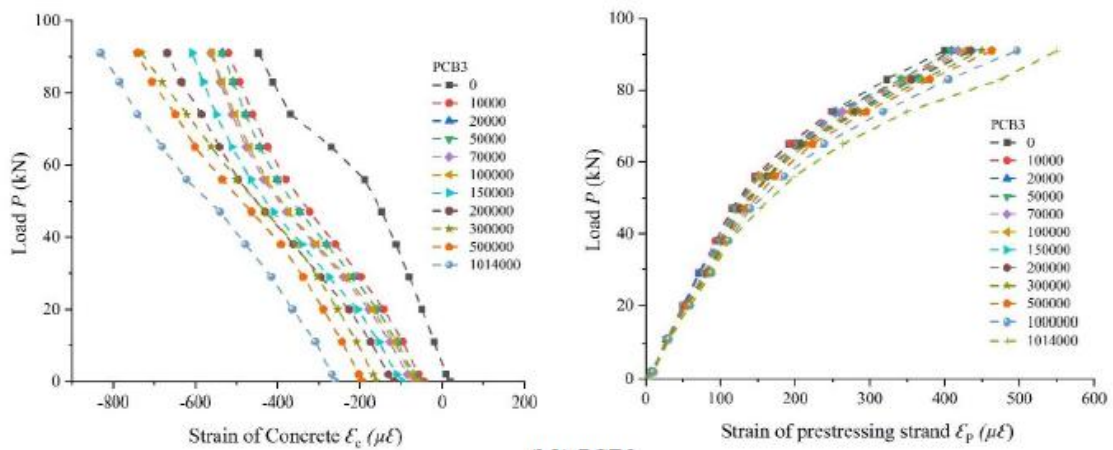
Fatigue test beam load-displacement curves depict in Fig.8. As the number of fatigue cycles increases, the load-displacement curve shifted in the direction of greater displacement. In the early and late stages of fatigue, the load-displacement curves were unevenly distributed, while at the medium stage of fatigue were denser. The slope of the load-displacement curve decreased as the number of cycles increased. This implies that the test beam was losing rigidity and softening. Progression of the major crack and the load-displacement curve, as shown in Fig.8 and comes with a three "S" form law. During the whole phase of PC beam fatigue process, the vertical cracks with a limited number and length occurred in the mid-pure span's bending region. The crack size was approximately 0.07 ~ 0.95 mm. Vertical cracks in the pure bending portion became larger and longer with time, and the number of cracks increased during the middle stage of fatigue. And around the loading points, the bending and shearing section developed oblique cracks. As the cyclic load was applied, the cracks opened and closed again, and the fractures on both sides of the beam were connected at the bottom. At this moment, the cracks' width, length, and number were all increasing. The major crack was 0.25 to 0.4 mm wide. Dynamic creep accumulated damage to the steel bar and prestressing strand during the fatigue process. The damage to the steel bar and prestressing strand accumulated throughout the fatigue process as a result of dynamic creep. When the bottom steel bar for beams PCB2 and PCB3 experiences tensile stress, and Strand wire for the beam PCB4 to PCB8 reached the critical point of tension, obvious dendritic oblique cracks appeared in the final stage of fatigue, for uncorroded beam PCB2 and less corroded beam PCB3, the steel bar fractured abruptly, resulting in significant increases in displacement and main crack width. The test beam had reached fatigue failure at this point. although the beam could still bear fatigue loads, but the external loads applied to the beam have greatly reduced. However, for beams with corroded prestressed strands, PCB4 to PCB8 wire fractured accrued prior to steel bar fracture during the middle and end stages of fatigue. The fatigue damage to the bottom tensile reinforcement and strand wire was steadily increasing, the fatigue failure of the PC beam was caused by the rapid fracture of the steel bar and prestressed wire.

### Strain development

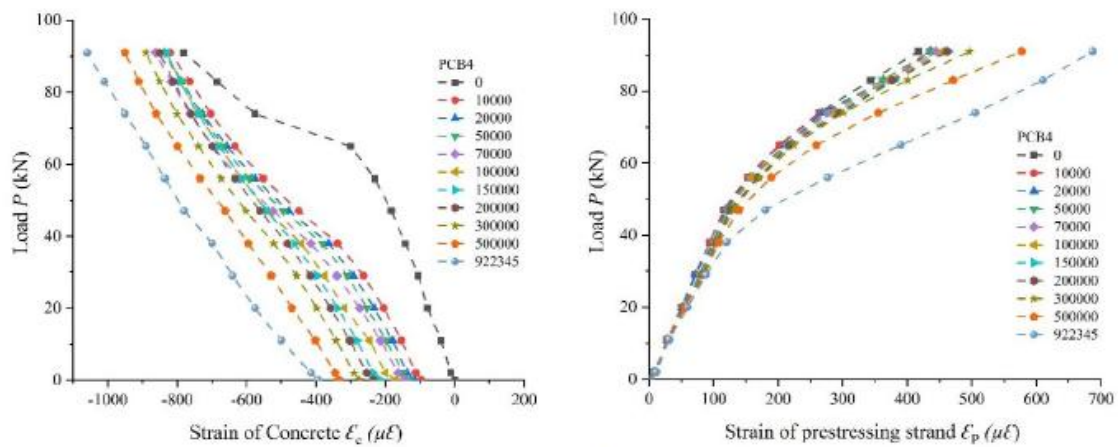
The load-strain curves of concrete in the compression zone, the bottom steel bar, and the prestressing strand under constant-amplitude fatigue loading are depicted in Fig 9 and 10. Tension is represented by positive strains, and compression is represented by negative strains. The effects of efficient prestress and test beam weight is taken into consideration when calculating the initial strain of concrete prior to fatigue loading. Through the test, strain is measured during the fatigue process. Concrete's strain-load curve can be determined by superimposing the two strains above. Due to construction conditions, certain steel bar strain gauges and prestressing strands were damaged. As a result, the pure bending region was picked for as much as feasible of the undamaged strain data. A zero value was assigned to each load-strain curve. Results of the tests indicated that concrete strains increased towards the direction of increased compressive strain. Furthermore, the slope of the steel bar and prestressing strand load-strain curves were steadily decreasing, and both steel bar and prestressing strand had plastic characteristics. Furthermore, the slope of the steel bar and prestressing strand load-strain curves were steadily decreasing, and both steel bar and prestressing strand displayed plastic characteristics. some of The strain gauges were damaged in the final stage of fatigue, preventing parts of the strain data from obtained.



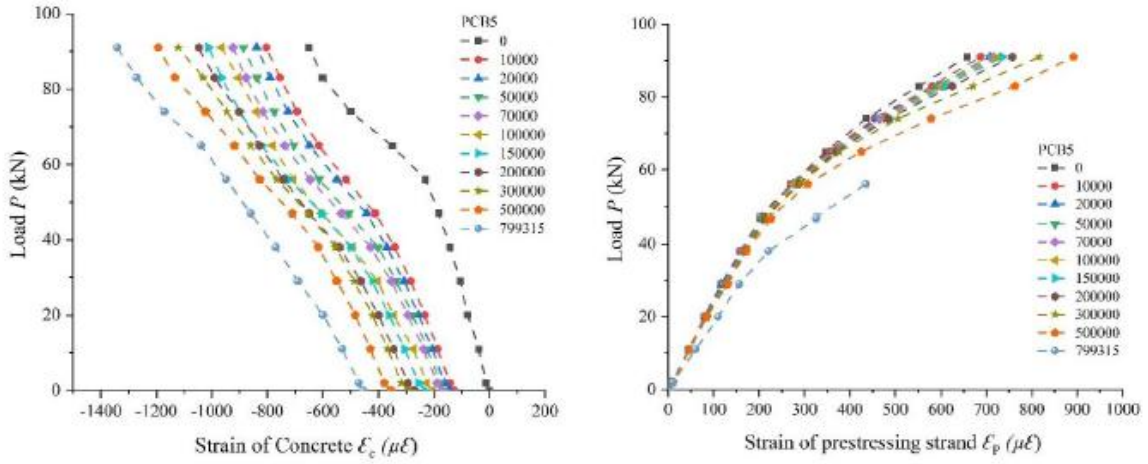
(a1) PCB2



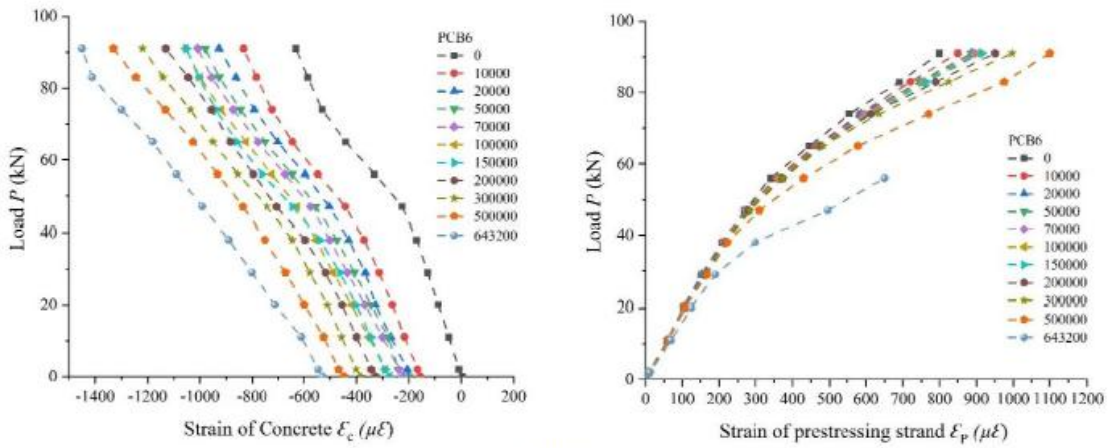
(b1) PCB3



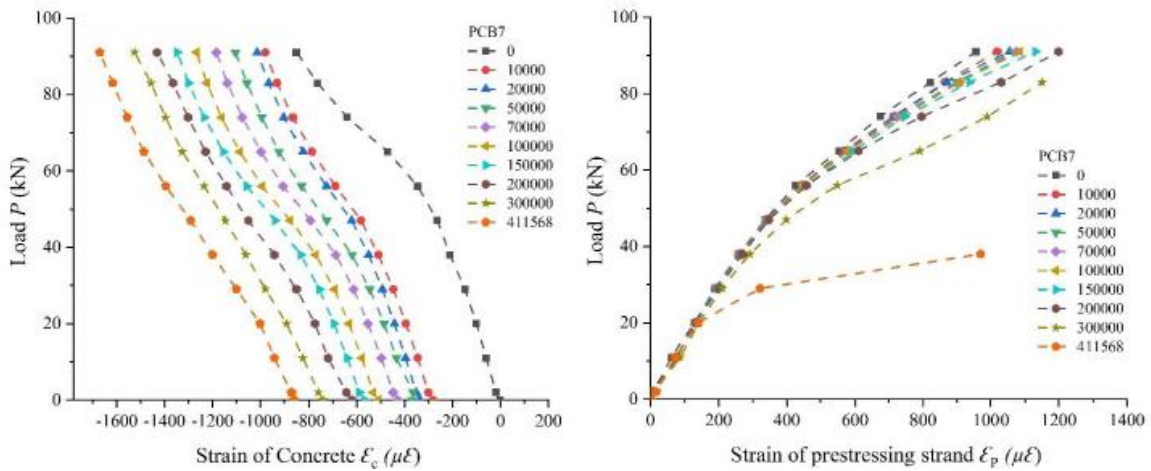
(c1) PCB4



**(d1) PCB5**



**(e1) PCB6**



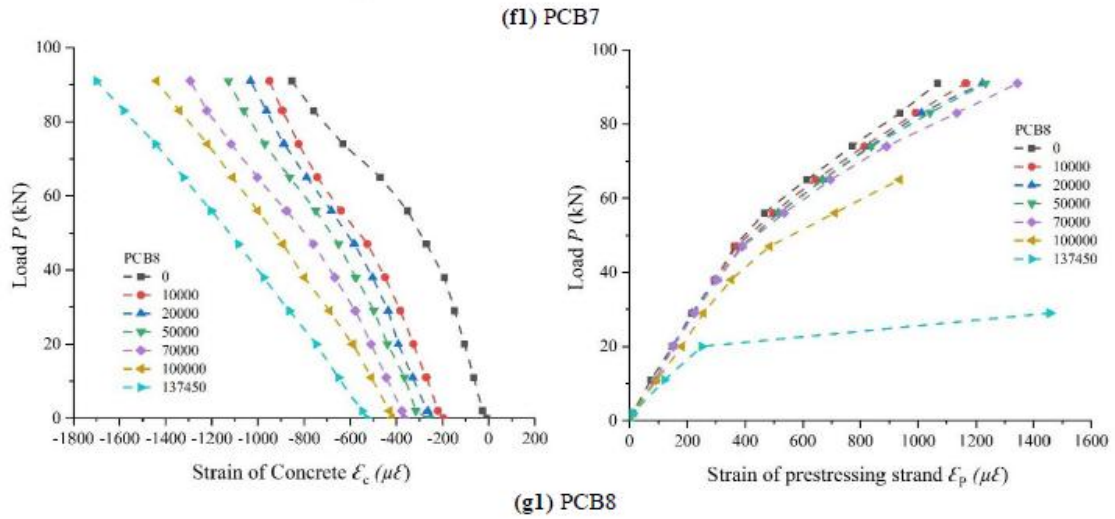
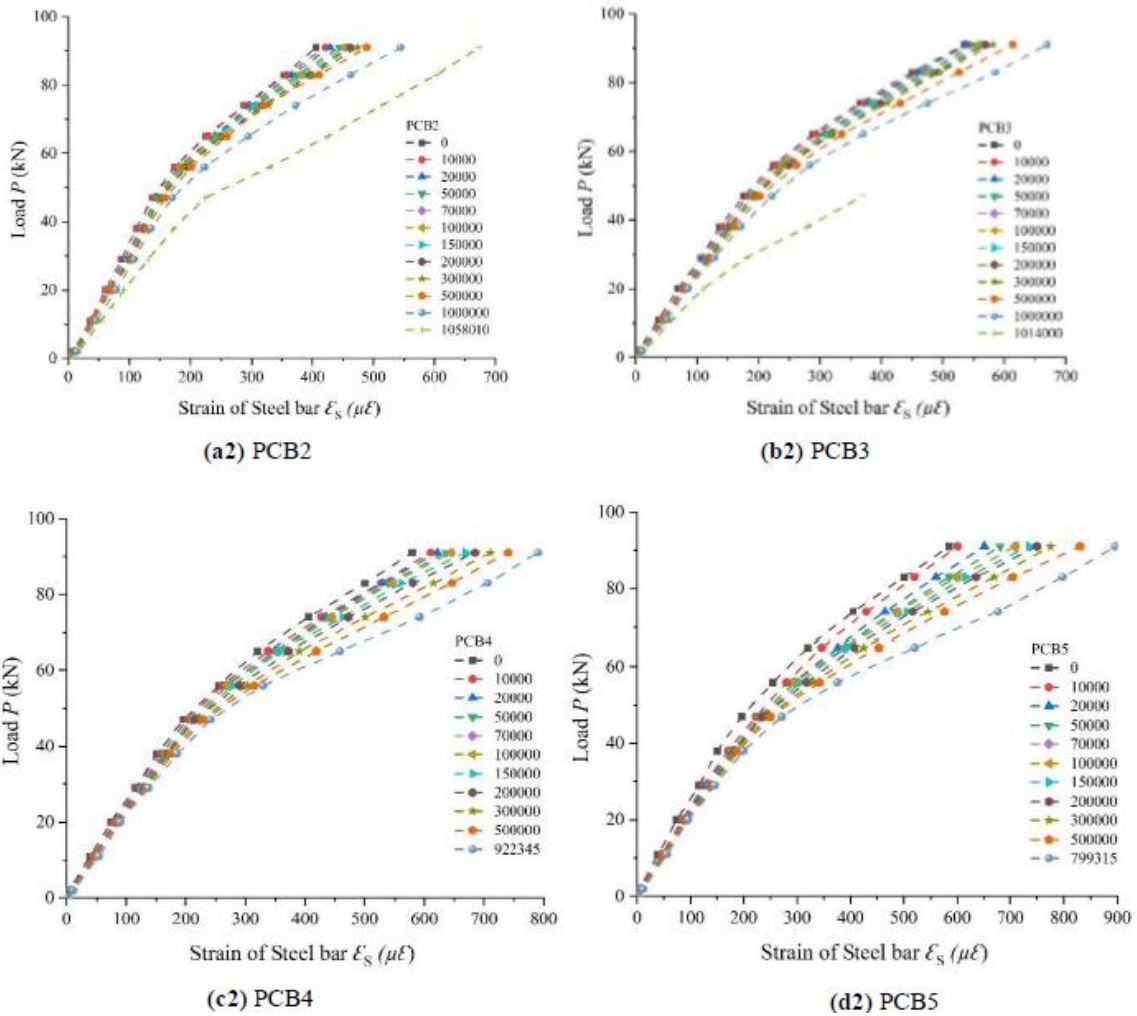


Fig. 9. Strain development of concrete, and prestressing strand under constant fatigue loading



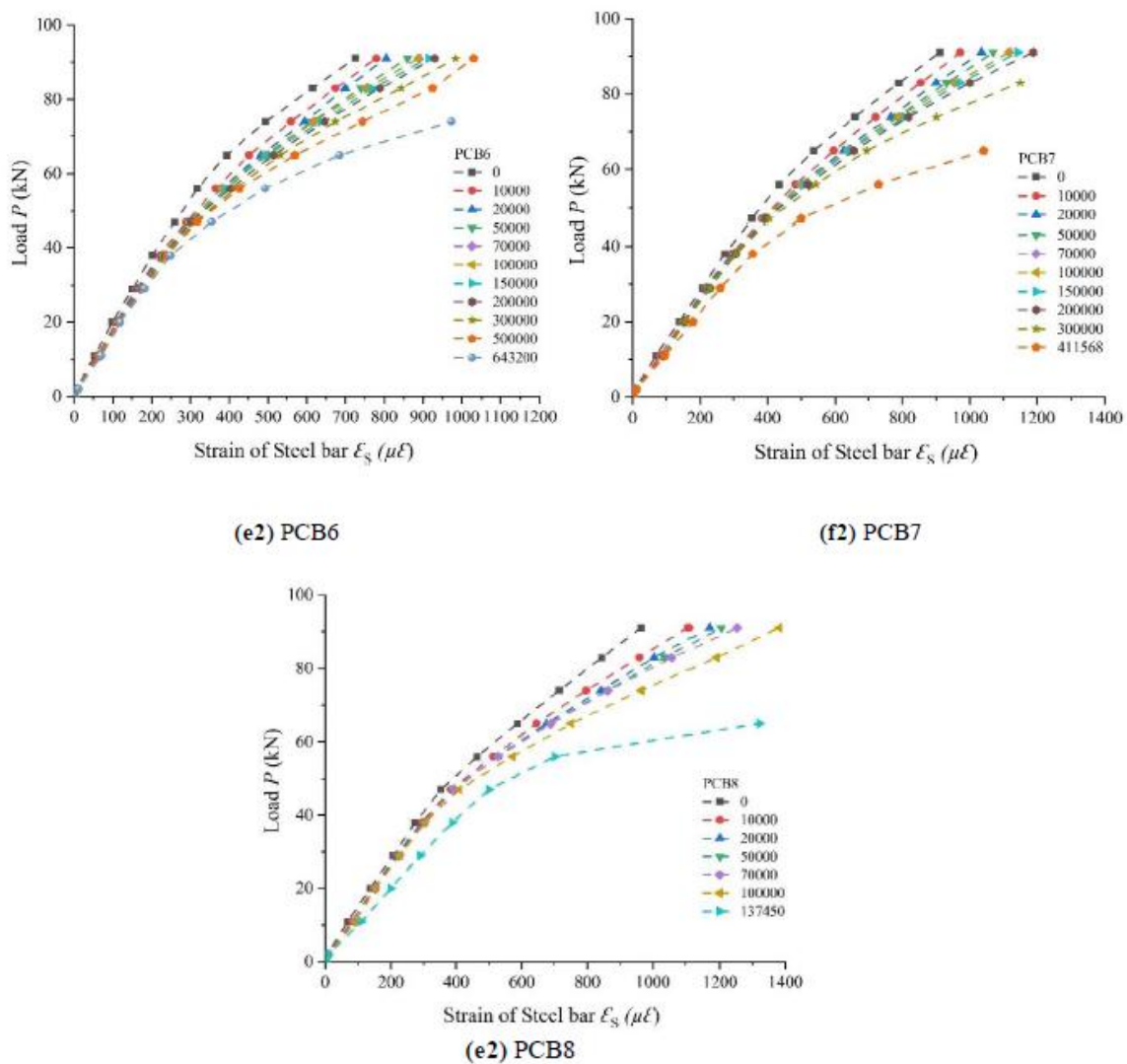


Fig. 10. Strain development of steel bar

#### IV. CONCLUSIONS

The purpose of this paper is to investigate experimentally the effects of corrosion-induced cracking and fatigue high cyclic loading on the performance of post-tensioned concrete beams. The following are the main conclusions:

Strand corrosion has an obvious negative impact on the fatigue behavior of PC beams. Corrosion has resulted in a loss of cross-sectional area of steel strands, which has significantly reduced the cyclic age.

When the corrosion loss of prestressing wires increases, the failure modes of beams change from longitudinal rebars to prestressing wires, in contrast to the uncorroded reference beams. However, the deflection, strain, and crack width increased at a faster rate as the prestressing wires corroded, and the outcome is consistent with the experimental evidence. The presence of strand corrosion exacerbates the displacement of the neutral axis and reduces the depth of concrete compression, and a significant reduction in beam ultimate strength and fatigue life span. In the current test, for instance, 30% corrosion loss reduces the fatigue life span of beams by approximately 61.1%.

Fatigue fractures of corrosion-corroded wire occur at the largest corrosion pit location, decreasing the stiffness of the PC beam significantly. After subjecting the beams to the same fatigue cycles, the stiffness of the PC beam is susceptible to the degree of corrosion-induced cracking, and corrosion induced cracking decreases the fatigue life of the PC beams comprehensively. Bond-behavior deterioration has minimal influence on the beams' fatigue life, although it does reduce flexural stiffness. Due to deterioration of bond behavior, the curvature of the section under fatigue load must be taken into consideration as well as the deflection of structures. Additionally, in contrast to the middle of the span, the corrosion of strands near the support seemed to have a slight impact on the overall behavior in the PC beam loading test.

### ACKNOWLEDGMENT

This research project was financially supported by the Science and technology project of the Hebei Provincial Department of transportation (YC-201912), China.

### REFERENCES

- [1]. Djeddi, L., et al., Reliability of acoustic emission as a technique to detect corrosion and stress corrosion cracking on prestressing steel strands. *International Journal of electrochemical science*, 2013. **8**(6): p. 8356-8370.
- [2]. Liu, X., et al., Degradation of mechanical behavior of corroded prestressing wires subjected to high-cycle fatigue loading. *Journal of Bridge Engineering*, 2017. **22**(5): p. 04017004.
- [3]. Zhang, W., et al., Fatigue behavior of corroded prestressed concrete beams. *Construction and Building Materials*, 2016. **106**: p. 198-208.
- [4]. Darmawan, M.S., Pitting corrosion model for partial prestressed concrete (PC) structures in a chloride environment. *IPTEK The Journal for Technology Science*, 2009. **20**(3).
- [5]. Herrmann, A.W. Asce 2013 report card for america's infrastructure. in IABSE symposium report. 2013. International Association for Bridge and Structural Engineering.
- [6]. Zhang, W.-p., et al., Variability in cross-sectional areas and tensile properties of corroded prestressing wires. *Construction and Building Materials*, 2019. **228**: p. 116830.
- [7]. Zhang, W., et al., Assessment of fatigue life for corroded reinforced concrete beams under uniaxial bending. *Journal of Structural Engineering* 2017. **143**(7): p. 04017048.
- [8]. Zhu, W., R.J.S. François, and I. Engineering, Prediction of the residual load-bearing capacity of naturally corroded beams using the variability of tension behaviour of corroded steel bars. *Structure and Infrastructure Engineering*, 2016. **12**(2): p. 143-158.
- [9]. Ma, Y., et al., Modeling constitutive relationship of steel bar removed from corroded PC beams after fatigue considering spatial location effect. *Journal of Materials in Civil Engineering* 2021. **33**(4): p. 04021019.
- [10]. Li, F., Y.J.C. Yuan, and B. Materials, Effects of corrosion on bond behavior between steel strand and concrete. *Construction and Building Materials*, 2013. **38**: p. 413-422.
- [11]. Lu, Z.-H., et al., Effect of chloride-induced corrosion on the bond behaviors between steel strands and concrete. *Materials and Structures*, 2021. **54**(3): p. 1-16.
- [12]. Wang, L., et al., Bond behavior between multi-strand tendons and surrounding grout: Interface equivalent modeling method. *Construction and Building Materials*, 2019. **226**: p. 61-71.
- [13]. Capozucca, R.J.C. and B. Materials, Detection of damage due to corrosion in prestressed RC beams by static and dynamic tests. *Construction and Building Materials*, 2008. **22**(5): p. 738-746.
- [14]. Zhang, W., et al., Probability distribution model for cross-sectional area of corroded reinforcing steel bars. *Journal of Materials in Civil Engineering* 2014. **26**(5): p. 822-832.
- [15]. Darmawan, M.S. and M.G.J.S.S. Stewart, Spatial time-dependent reliability analysis of corroding pretensioned prestressed concrete bridge girders. *J Structural Safety*, 2007. **29**(1): p. 16-31.
- [16]. Zhang, W., et al., Assessment of fatigue life for corroded reinforced concrete beams under uniaxial bending. *Journal of Structural Engineering*, 2017. **143**(7): p. 04017048.
- [17]. Li, F., et al., Pitting damage characteristics on prestressing steel strands by combined action of fatigue load and chloride corrosion. *Journal of Bridge Engineering*, 2017. **22**(7): p. 04017023.
- [18]. Li, F., Y. Qu, and J.J.E.F.A. Wang, Bond life degradation of steel strand and concrete under combined corrosion and fatigue. *Engineering Failure Analysis*, 2017. **80**: p. 186-196.
- [19]. Liu, X., et al., Degradation of mechanical behavior of corroded prestressing wires subjected to high-cycle fatigue loading. *ASCE*, 2017. **22**(5): p. 04017004.
- [20]. Zhang, W., et al., Fatigue behavior of corroded prestressed concrete beams. *Construction Building Materials* 2016. **106**: p. 198-208.
- [21]. Xin, Q., et al., Fatigue Behavior of Prestressed Concrete Beams under Overload. *Journal of Engineering Science Technology Review* 2017. **10**(4).
- [22]. Yu, F., et al. Fatigue behavior of prestressed concrete beams under corrosion. in *Advanced Materials Research*. 2011. Trans Tech Publ.
- [23]. Yuan, H., et al., Corroded reinforced concrete beams under low-speed and low-cycle fatigue loads. *J Construction Building Materials* 2018. **186**: p. 644-651.
- [24]. Sun, J., et al., Performance deterioration of corroded RC beams and reinforcing bars under repeated loading. *J Construction Building Materials* 2015. **96**: p. 404-415.
- [25]. El Maaddawy, T.A. and K.A.J.J.o.m.i.c.e. Soudki, Effectiveness of impressed current technique to simulate corrosion of steel reinforcement in concrete. *J Journal of materials in civil engineering* 2003. **15**(1): p. 41-47.

***Corroded Post-Tensioned Concrete Beams Fatigue Behaviour Under High Cyclic Loading***

- [26]. Rinaldi, Z., et al., Experimental evaluation of the flexural behavior of corroded P/C beams. J Construction Building Materials 2010. **24**(11): p. 2267-2278.
- [27]. Shahawi, M.E. and B.d.J.J.o.S.E. Batchelor, Fatigue of partially prestressed concrete. J Journal of Structural Engineering 1986. **112**(3): p. 524-537.
- [28]. structures, C.f.d.o.c.,” GB 50010-2002. .

Your Name	Photo	E-mail address & Affiliation	Title*	Research Field
Mohammad Mahdi Sultani		<a href="mailto:mahdi2.su@gmail.com">mahdi2.su@gmail.com</a>	Master student	Prestressed concrete and Bridge Engineering
Liang Dong		13622114075@139.com	full professor	Bridge Engineering
Ge Changwei		244106948@qq.com	Master student	Bridge Engineering

Mohammad Mahdi Sultani, et. al. "Corroded Post-Tensioned Concrete Beams Fatigue Behaviour Under High Cyclic Loading." *IOSR Journal of Engineering (IOSRJEN)*, 12(03), 2022, pp. 01-15.